Controlling the Photonic Properties of Cholesteric Cellulose Nanocrystal Films with Magnets

Bruno Frka-Petesic,* Giulia Guidetti, Gen Kamita, and Silvia Vignolini*

The self-assembly of cellulose nanocrystals is a powerful method for the fabrication of biosourced photonic films with a chiral optical response. While various techniques have been exploited to tune the optical properties of such systems, the presence of external fields has yet to be reported to significantly modify their optical properties. In this work, by using small commercial magnets (≈ 0.5–1.2 T) the orientation of the cholesteric domains is enabled to tune in suspension as they assemble into films. A detailed analysis of these films shows an unprecedented control of their angular response. This simple and yet powerful technique unlocks new possibilities in designing the visual appearance of such iridescent films, ranging from metallic to pixelated or matt textures, paving the way for the development of truly sustainable photonic pigments in coatings, cosmetics, and security labeling.

The increasing need of multifunctional materials with well-controlled properties can be met by adopting self-assembly strategies relying on biosourced nanosized building blocks. Such approaches can offer a cost-effective and scalable solution to design materials with a desired optical response.[1] Cellulose nanocrystals (CNCs) are an excellent example of such a biosourced nanomaterial, owing to a unique combination of chemical, mechanical, and optical properties,[2,3] which explains the increase of interest in this system for applications as pigments,[4] security coatings,[5,6] sensing or responsive materials,[7–12] and mesoporous chiral nanotemplates.[13–15]

Colloidal suspensions of CNCs exhibit a cholesteric liquid crystalline behavior above a threshold concentration[16–20] that can be retained upon solvent evaporation to form dry films that display a strong photonic response. In particular, such films behave as standard cholesteric Bragg reflectors[14] whose optical response is determined by their helix axis, $\mathbf{m}$, and pitch, p.[21]

For these systems, the control of the pitch, and therefore the reflected wavelengths, can be successfully achieved by adjusting

Dr. B. Frka-Petesic, G. Guidetti, Dr. G. Kamita,
Dr. S. Vignolini
Melville Laboratory for Polymer Synthesis
Department of Chemistry
University of Cambridge
Cambridge, Lensfield Road, CB2 1EW, UK
E-mail: bf284@cam.ac.uk; sv319@cam.ac.uk

a variety of parameters.[22–29] However, the orientation of the helix axis $\mathbf{m}$ in such films has been limited only by the specific geometrical conditions in which self-assembly occurs. Therefore, the manipulation of the orientation of the helix $\mathbf{m}$ has so far not been addressed, or was at best limited to favor its vertical orientation uniformly across the sample.[28,30,31] While the use of external fields, such as electric[32–34] and magnetic,[29,35–50] have been shown to provide a powerful control over the CNC orientation in suspensions, they have been so far considered impractical as a tool to tailor the photonic properties of the films. More specifically, it has been believed for over two decades that the magnetic orientation of the cholesteric phase in CNC suspensions required always very strong fields (≥5 T), which probably discouraged many from investigating this method, due to the seemingly limited applicability and thus relevance of this technique to produce useful aligned CNC-based materials. The alignment of CNCs under more accessible fields (≤1 T, e.g., with a pair of neodymium magnets) is indeed much more desirable for practical applications, but an attempt reported by Pan et al. using 0.2 T led to no significant control over the helix orientation.[29] The orientation of cholesteric suspensions in magnetic fields is due to the intrinsic anisotropic diamagnetic susceptibility of the individual CNC,[49] and their orientation in low magnetic fields (0.56–1.2 T) is due to a cooperative effect in their cholesteric arrangement, as first reported by Kimura et al.[41] on cholesteric suspensions of micron-long tunicate nanofibrils, and only recently quantified on much shorter cotton-sourced CNCs by De France et al.[50] To our knowledge, such conditions have been successfully exploited only in rheological studies[51] and reinforced nanocomposite papers.[52]

In this work, we report the use of commercial neodymium (NdFeB) magnets as a powerful and versatile tool to control the orientation of the cholesteric domains and to produce colored CNC films with unique control over their final optical properties. To achieve this, the suspension is evaporated in the immediate vicinity of NdFeB magnets, so that the local magnetic field perceived by the drying suspension induces a long-range order of the cholesteric phase, which is subsequently retained in the solid-state. By adjusting the spatial configuration of the magnet(s) with respect to the drying suspension, we are able to produce solid nanostructured films with improved uniformity in the orientation of the cholesteric axes, leading to large homogenous films, and especially to control its orientation. **Figure 1** illustrates examples of the striking controllable optical effects obtained with this technique; here a selection of macroscopic images of chiral cellulose films cast using different

**ADVANCED
SCIENCE NEWS**

www.advancedsciencenews.com
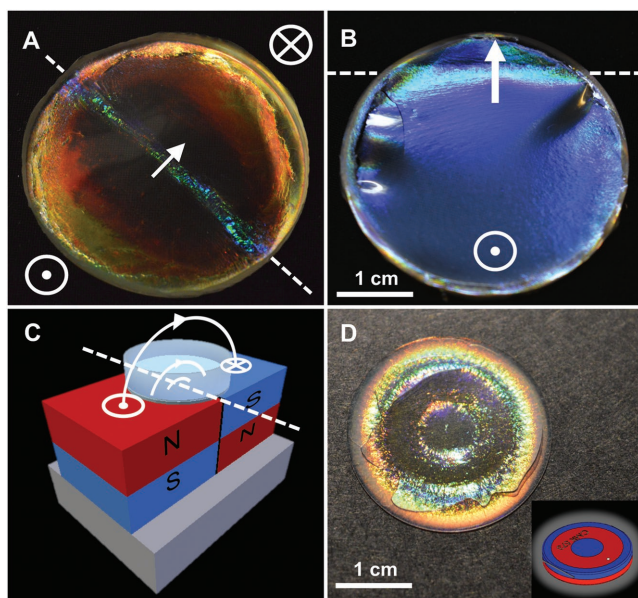
**ADVANCED
MATERIALS**

www.advmat.de

Figure 1. Films obtained from the slow evaporation of an aqueous suspension of CNCs in a dish placed over NdFeB magnets. A,B) Examples of films that were cast spanning two magnets, as indicated by the schematic in (C). D) Exotically patterned films can be obtained when casting on a patterned polydomain magnet (Polymagnet) displaying opposite magnetization direction on the same face (the inset shows a schematic of the templating polymagnet).

magnets are shown. It should be noted that large magnets, as employed in Figure 1B, were preferred when casting films on extended surfaces, but we also demonstrated this effect using smaller magnets as well as a patterned Polymagnet to locally template the optical properties of smaller portions of films with the same efficiency (cf. Figure 1D and Figure S6, Supporting Information). While other templating methods have also been reported for CNC films, such as local temperature gradients,[53] local substrate variation,[54] or multisteps casting,[55] these magnetically templated films present both enhanced optical contrast and unique angular response properties.

To better understand how the presence of a magnetic field affects the self-assembly of the CNCs, we cast the same starting suspension under the same conditions of temperature and humidity for three different magnetic environments ([CNC] = 8.5 wt%, [NaCl] = 8.5×10^{-3} M, Section A and Figures S1–S4, Supporting Information): in the absence of a magnet (control sample), in a homogeneous vertical magnetic field, and at the junction between two magnets placed side-by-side, to obtain a highly tilted magnetic field near their junction (Figure 1C and Figure S5, Supporting Information).

The three obtained dry films display striking differences visible by naked eye, as shown in Figure S6 (Supporting Information). The reported photographs of the three samples were taken under the same illumination conditions, and highlight how the scattering response of the samples changes for the different magnetic field configurations. Similar observations are reported for different suspensions, with varying ratios of NaCl:CNC (Figure S7, Supporting Information).

To capture the unusual angular dependence of the optical response, the films were systematically analyzed by angular resolved optical spectroscopy.[56,57] With this technique, a collimated white light beam illuminates the sample at a defined angle and the scattering response from the sample is collected across a wide range of angles. The comparison of the three samples (no field, vertical, and tilted magnetic fields) is summarized in **Figure 2**. Scattering plots in Figure 2A–C and Figure 2D–F report the intensity of the reflected light in $\log_{10}$-scaled black–blue–yellow colors for different angles of collection and for an angle of incident of 0° and −30°, respectively.

The optical response of these films relies on the fact that the CNC rods are locally aligned with their long axis along a director **n** that rotates at the sub-micrometer scale and describes a left-handed helix, characterized by its helix axis **m** and its pitch p, the latter being defined as the distance separating rods of the same orientation after a 360° rotation.[21] The structural color of the film arises from the diffraction of the incident light, which locally obeys the Bragg law inside the film, $\lambda = n\,p\,\cos\theta'$, where λ is the wavelength of the reflected light, n is the average optical index, and θ' is the angle defined locally between the incident light and the helix axis **m**. As a result, the nonuniform orientation of the helix **m** in polydomains films contributes to their pixelated and rainbow-like appearance.[58]

As shown in Figure 2A,D, the films prepared without any magnet display a broadened angular wavelength response, indicating a broad distribution of orientations of cholesteric structures inside the film. In this case, the homeotropic anchoring of **m** on the top and bottom interfaces is favorable to the vertical alignment of the cholesteric structure, but in practice such effect has a limited efficiency throughout the film thickness.[28]

By contrast, films assembled in the presence of the magnetic field can enhance the intensity of the reflected light only for a selected range of angles. Specifically, for a vertical magnetic field, the film shows a strong specular reflection (i.e., $\theta_{out} = |\theta_{in}|$, Figure 2B,E), in the direction perpendicular to the sample surface, indicating that the cholesteric structure is well aligned throughout the film with **m** oriented normal to the film surface. Even more interestingly, the sample dried in a tilted magnetic field displays a strong reflection at an angle of $\theta_{out} \approx |\theta_{in}| + 12°$ with respect the normal of the sample surface ($\theta_{out} \neq |\theta_{in}|$, Figure 2C,F). These observed optical responses suggest an underlying cholesteric structure for each sample that is summarized in the schematics of Figure 2G–I.

The effect of the magnetic field applied upon drying is further analyzed using polarized optical microscopy, as reported in **Figure 3**. Polarization resolved reflection images of the three previous samples were collected in bright field and dark field configuration in order to distinguish the polarization features of their local optical response.[56] A Bertrand lens was then used to further image the full scattering response in k-space.

The sample prepared in the absence of a magnetic field displays signal in both left- and right-handed circular polarization and in both bright and dark field configurations due to the presence of highly tilted cholesteric domains (Figure 3A,E). This broad and polychromatic angular response is confirmed by the observations in k-space (Figure 3I) and is in good agreement with films containing highly tilted domains.[59]

By contrast, samples prepared under magnetic fields reflect predominantly left-handed polarized light in bright field with little scattered light observed. For vertically aligned fields mostly blue light is reflected at normal incidence in bright
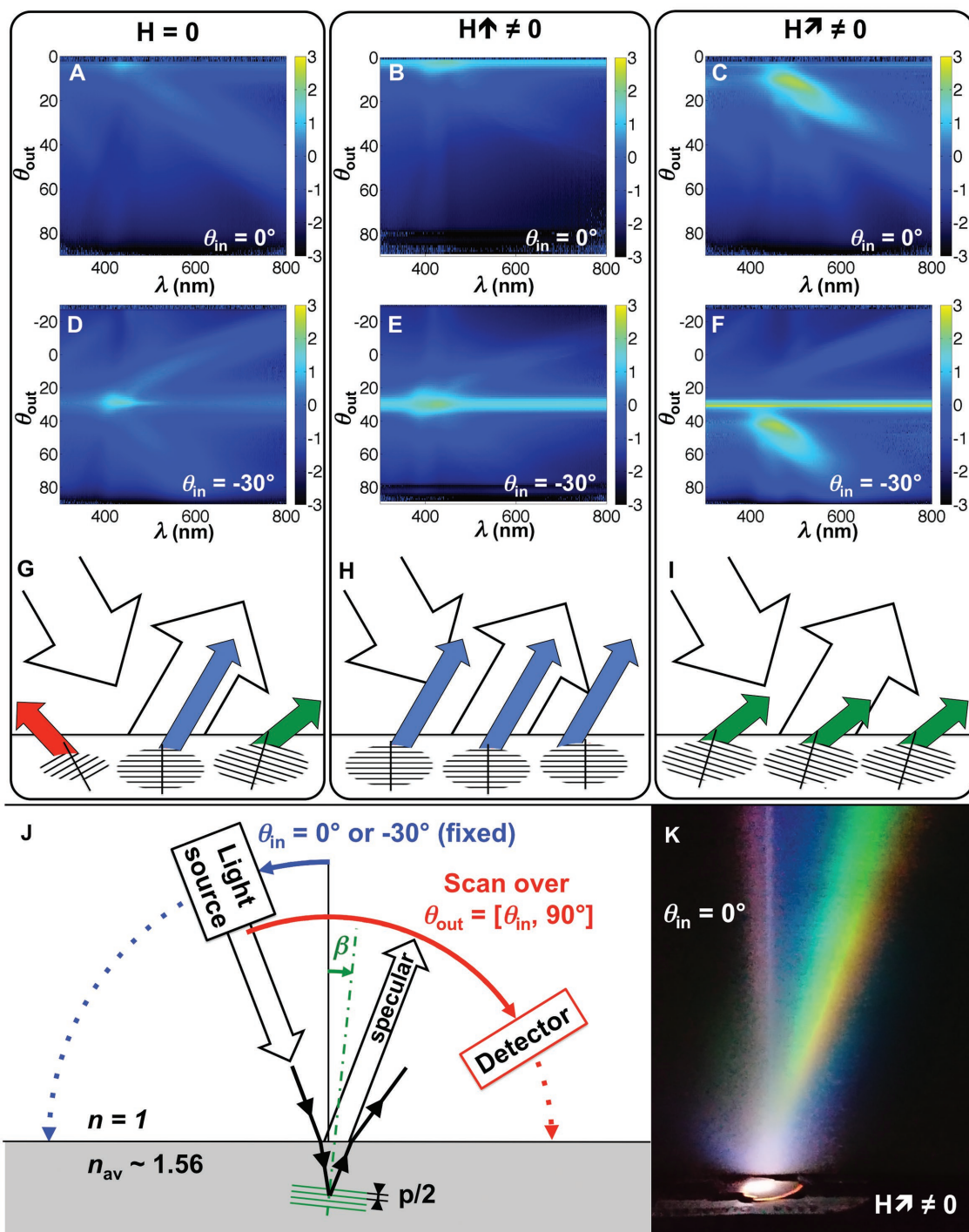
ADVANCED
SCIENCE NEWS
www.advancedsciencenews.com

ADVANCED
MATERIALS
www.advmat.de

Figure 2. Angular resolved optical spectroscopy of CNC films assembled under three different conditions: no field (**H** = 0), vertical (**H↑** ≠ 0), and tilted magnetic field (**H↗** ≠ 0, measured in position x = +2.5 mm, cf. axes definition in Figures S6C and S13B, Supporting Information). The intensity of the light diffracted by the sample is reported in $\log_{10}$-scale with its spectral composition (i.e., wavelength λ) for each angle of detection (θ_{out}) when the probing incident light is either normal (θ_{in} = 0°, A–C) or tilted (θ_{in} = −30°, D–F). A model fitting the data is proposed in Figure S15 (Supporting Information). G–I) Schematics of the orientation of the cholesteric nanostructures responsible for the observed optical response (white arrows symbolize white incident light and specular reflection). J) Schematic of the goniometer and definition of the angles θ_{in} and θ_{out}. K) Photograph of the off-specular response of a film with a tilted cholesteric structure. For the sake of clarity, the incident and diffracted light beams are grazing a screen placed in the background of the diffraction plane.

field with a net contrast between left- and right-handed circular polarization, as expected only for vertically aligned domains (Figure 3B,F,J). For a tilted magnetic field, the contrast between left and right decreases (Figure 3C,D) and the diffracted light is reflected off-line with a clear red-shift (Figure 3K,L), that becomes more apparent in dark field (Figure 3G,H).
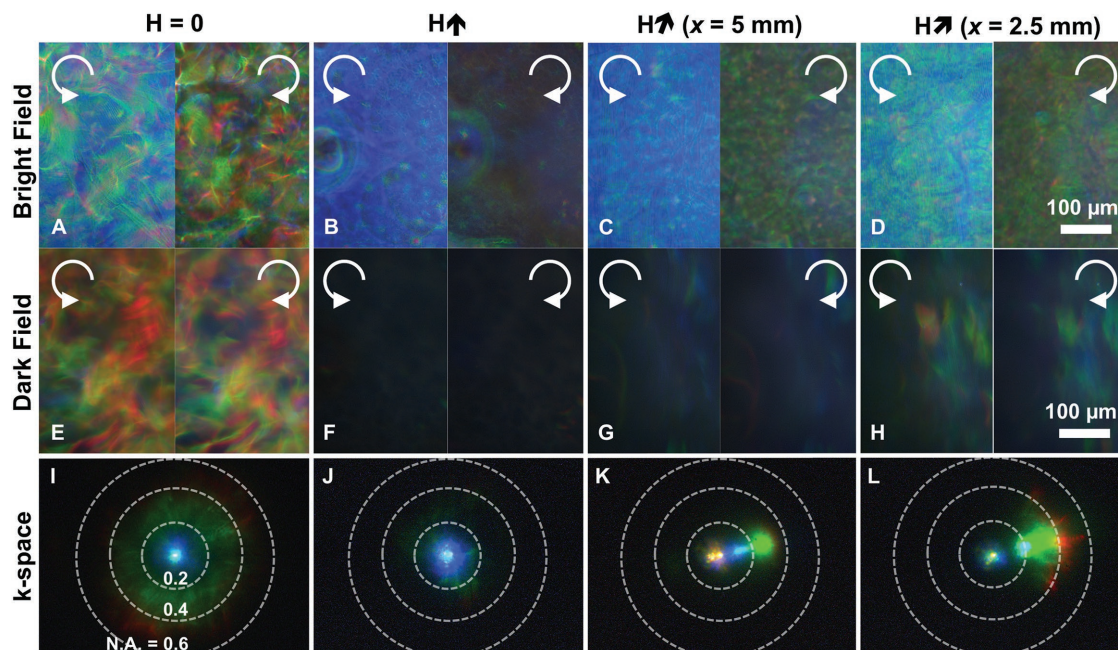
Figure 3. Polarized optical images of films prepared in zero field (**H** = 0, far left), in vertical field (**H**↑), and for two increasingly tilted magnetic fields (**H**↗). The films were analyzed in A–D) bright field and E–H) dark field, respectively, using either a left- (↺) or right-circularly polarized filter (↻), and I–L) in *k*-space, as imaged with a Bertrand lens.

To reveal the influence of the magnetic field on the internal cholesteric arrangement of the CNC films, their cross-section is investigated using scanning electron microscopy (SEM),[60] as reported in **Figure 4**. The film prepared without magnetic field shows clearly a polydomain structure: the orientation of the cholesteric domains is less controlled (Figure 4A). By contrast, the film prepared under a vertical magnetic field seems perfectly monodomain and highly uniform in both orientation and pitch (Figure 4B), although some disclinations remain visible. Similarly, the film prepared in presence of a tilted magnetic field (Figure 4C) displays locally a homogeneous cholesteric monodomain but with a clear tilt with respect to the film–air interface, explaining the unusual optical angular response. We found no previous example of such control of the cholesteric tilt in the literature. Different magnifications are presented in Figure S10 (Supporting Information) and a further film with extremely tilted regions ($\beta_f \approx 17°$) is presented in Figure S11 (Supporting Information).

Surprisingly, the film structure in the area dried directly above the junction between the two magnets displays a clear zig-zag pattern (Figure 4D, more examples in Figures S11–S13, Supporting Information). We interpret this pattern as the result of mechanical buckling of the cholesteric structure upon unidirectional vertical compression perpendicularly to its helix axis **m**. The vertical compression is expected to play an important role in this drying geometry (i.e., the solvent evaporates from the top while the surface area is kept constant) from the moment the drying suspension reaches a threshold concentration where the kinetic arrest occurs and the mutual orientation of the rods cannot relax anymore.[61–64]

These undulations are fundamentally different from the Helfrich–Hurault or related instabilities[65–68] observed in confined cholesterics under the influence of external fields coupling parallel to the local director **n**. So far we observed similar buckling waves only in a spherical microdroplet geometry,[62] and is consistent with a lower compressibility of the cholesteric structure normal to **m**, which is expected in this system.[63]

While we clearly demonstrate that casting CNC suspensions on NdFeB magnets does successfully induce an alignment of the cholesteric structure in the final film, it would be misleading to conclude that the final alignment in the dry film corresponds to the local direction of the magnetic field applied during casting. Indeed, the vertical compression upon drying is expected to affect the final tilt of the cholesteric nanostructures. To clarify this point, we compared the observed tilt of the cholesteric structures in the films with the local tilt of the magnetic field at the same position during the casting. For this purpose, the magnetic field was mapped experimentally and further computed to expand its local tilt across the whole sample cross-section (Section D and Figures S11 and S12, Supporting Information). We found that the tilt of the cholesteric structures is always much smaller than the corresponding tilt of the magnetic field. For instance, we measured a final tilt, β_f of ≈4°–6° (defined from the vertical axis) in a position ($x = 2.5$ mm) where we measured the field to be 65°–70°, i.e., rather horizontal than vertical.

To account for the distortion of the cholesteric structure upon vertical compression, we use a simple compression model adapted from Ericksen–Leslie theory[57,69] (details in Section E, Supporting Information). Our simplified model allows capturing the linear deformation expected from an assembly of cholesteric domains of identical pitch and purely randomized orientations. Neglecting any mechanical anisotropy that could explain the observed buckling, this purely geometrical model
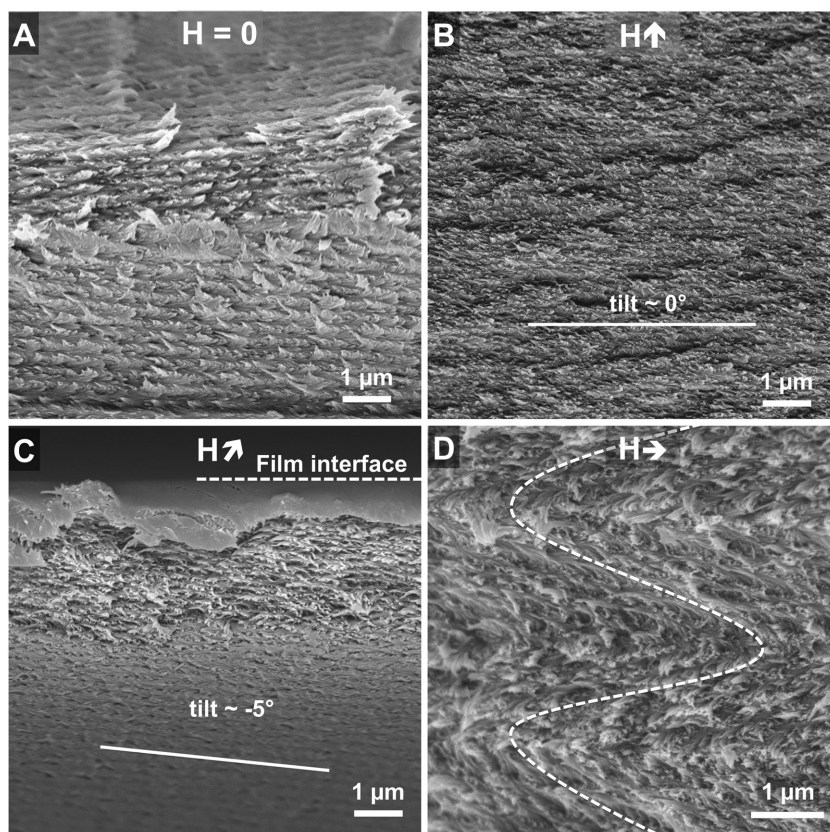
**ADVANCED
SCIENCE NEWS**

www.advancedsciencenews.com

**ADVANCED
MATERIALS**

www.advmat.de

Figure 4. Scanning electron microscopy (SEM) of the cross-sections of CNC films prepared: A) in absence of magnetic field (**H** = 0), B) in a vertical magnetic field (**H**↑), C) in a tilted magnetic field (**H**↗), and D) in a nearly horizontal field (**H**→). While the absence of a magnetic field leads to a cholesteric polydomain structure with various tilts and pitches, the application of such magnetic field upon drying leads to a homogeneous pitch and orientation in either vertical or tilted direction (see Figure S10 of the Supporting Information for different magnifications), while a perfectly horizontal field leads to more complex zig-zag patterns indicating buckling phenomena (see Figures S11–S13 of the Supporting Information for further examples).

transition.[73,74] Such transition is characterized by a magnetic field threshold required to tilt the liquid crystalline alignment, while the resulting alignment profile is usually given by a compromise between both conditions and the minimization of the director distortion. We believe that the anchoring will get stronger upon further drying as the vertical confinement increases,[62,75] contingent that it occurs before the sample becomes kinetically arrested. This can cause a complex self-assembly behavior upon drying that could impact the tilt of the final cholesteric structure.

To conclude, we have shown that the magnetic fields generated by common NdFeB magnets can be used to achieve unprecedented control over the self-assembly of cellulose nanocrystals into colorful films. We demonstrate an improved homogeneity of the cholesteric pitch and orientation and, more importantly, the possibility to specifically orient the cholesteric structure either vertically or away from the usual planar orientation into specific directions. In this latter case, the resulting tilted structures reflect selected wavelengths off-specularly from the air–film interface, enabling a complete separation of their chiroptical response from the unspecific light reflected at the air–film interface.

Controlling the orientation of the cholesteric helix is fundamental to the design of the angular optical response of cellulose-based films. The helix orientation directly impacts the visual appearance of the films and therefore their use in coatings and cosmetics. Furthermore, gaining control over the directionality of the photonic response uniquely enables the design of complex optical properties that could encode in the same film different scattering and polarization features, e.g., for security labeling applications. Finally, the simplicity of this method to improve the homogeneity of CNC-based nanostructured films suggests that it could be of benefit to all applications where high quality optical or mechanical properties are desired, such as sensors or nanotemplating agents.

predicts the final tilt β_f and pitch p_f of the structure for an initial tilt β_i and pitch p_i, and a macroscopic compression ratio α ($0 < \alpha < 1$), corresponding roughly to the volume fraction of the suspension at the kinetic arrest. Interestingly, this model also captures the increase of the pitch as the tilt increases (Figure 4B–D), which, in turns, using Bragg's and Snell laws,[57,70,71] explains the observed red-shift of the scattering at higher angles (Figures 2A,D and 3I–L and Figures S16 and S17, Supporting Information). Indeed, a small blue-shift would be otherwise expected from a film with a constant pitch distributed along various directions,[57] which validates our model.

Exploiting this approach, we find that the calculated initial tilt β_i of the domains is still significantly lower ($\beta_i \approx 20°–30°$) than the corresponding tilt of the magnetic field ($\beta_H \approx 65°–70°$) where they were observed. The mismatch between these two tilt values indicates that other phenomena also play an important role in defining the initial alignment β_i of the cholesteric domains under magnetic field. Indeed, mechanisms such as tactoid coalescence and relaxation of the cholesteric orientation have been reported recently.[30,36,72] Moreover, the alignment of cholesteric fields under both external fields and conflicting anchoring conditions usually involves a Fréedericksz

Experimental Section

Cellulose Nanocrystals Suspension: Cellulose nanocrystals were obtained from acid hydrolysis[76] of Whatman No. 1 cellulose filter paper (30 g) with sulfuric acid (64 wt%, 420 mL) at 66 °C for 30 min, before quenching with deionized ice and water and purification by centrifugation and dialysis against deionized water (described in more detail in Section A, Supporting Information). The suspension was then tip-sonicated, vacuum-filtered, and finally concentrated to 14.5 wt% with an osmotic bath of poly(ethylene glycol) (35 kDa). This constituted the starting batch. Unless otherwise specified, the films presented in this work were obtained by dilution with milli-Q water and sodium chloride

(0.1 M) with a fixed [NaCl]/[CNC] ratio of 100 mmol kg^{-1}. The imaging of the rods by atomic force microscopy, their conductometric titration,[77] and their phase diagram are presented in the Supporting Information (Section A and Figures S1–S3, Supporting Information).

NdFeB Magnets: Two types of nickel-plated neodymium magnets (NdFeB) were used. Except where otherwise specified, large rectangular magnets (ref. F390-N42, N42 grade, (*x*, *y*, *z*) dim. L40 × W40 × H30 mm^3, First4magnets) with magnetization along *z*-axis were used (Figure S10, Supporting Information). The magnetic field close to their upper surface was experimentally measured (Figure S14, Supporting Information) and further calculated (Figure S15, Supporting Information) throughout the sample cross-section. An additional small disk-shaped magnet (ref. 1000573, Polymagnet) with a patterned concentric magnetization was used to further demonstrate the local control over the cholesteric alignment (Figure 1 D and Figure S8, Supporting Information).

Film Fabrication: Starting aqueous CNC suspension ([CNC] = 14.5 wt%) was diluted with milli-Q water and NaCl 0.1 M to reach [CNC] = 8.5 wt% at a fixed [NaCl]/[CNC] ratio and was homogenized with a vortex stirrer. The suspension was then placed in a petri dish (35 mm nontreated PS, ref. 430588, Corning, VWR) and left drying while covered with an open plastic lid in ambient conditions (*T* ≈ 22 ± 2 °C, RH ≈ 30% ± 5%, with a drying time on the order of a week, cf. Figure S4, Supporting Information). Magnetic fields were applied to drying suspension by placing the dishes in immediate vicinity of the magnet(s), as described in Figures S5, S14, and S15 (Supporting Information).

Characterization: The samples optical and structural properties were investigated using different settings, including direct observation, angular resolved optical spectroscopy, polarized optical microscopy, and scanning electron microscopy, as described in more detail in the Supporting Information.

Supporting Information

Supporting Information is available from the Wiley Online Library or from the author. Open Data are available on the Cambridge repository at the address: https://doi.org/10.17863/CAM.9517.

Conflict of Interest

The authors declare no conflict of interest.

[1] A. G. Dumanli, T. Savin, *Chem. Soc. Rev.* **2016**, *45*, 6698.

[2] Y. Habibi, L. A. Lucia, O. J. Rojas, *Chem. Rev.* **2010**, *110*, 3479.

[3] N. Grishkewich, N. Mohammed, J. Tang, K. C. Tam, *Curr. Opin. Colloid Interface Sci.* **2017**, *29*, 32.

[4] R. Bardet, F. Roussel, S. Coindeau, N. Belgacem, J. Bras, *Carbohydr. Polym.* **2015**, *122*, 367.

[5] Y. P. Zhang, V. P. Chodavarapu, A. G. Kirk, M. P. Andrews, *J. Nanophotonics* **2012**, *6*, 063516.

[6] C. Chindawong, D. Johannsmann, *J. Appl. Polym. Sci.* **2014**, *131*, 41063.

[7] Y. P. Zhang, V. P. Chodavarapu, A. G. Kirk, M. P. Andrews, *Sens. Actuators, B* **2013**, *176*, 692.

[8] J. A. Kelly, A. M. Shukaliak, C. C. Y. Cheung, K. E. Shopsowitz, W. Y. Hamad, M. J. MacLachlan, *Angew. Chem., Int. Ed.* **2013**, *52*, 8912.

[9] T.-D. Nguyen, W. Y. Hamad, M. J. MacLachlan, *Adv. Funct. Mater.* **2014**, *24*, 777.

[10] A. Espinha, G. Guidetti, M. C. Serrano, B. Frka-Petesic, A. G. Dumanli, W. Y. Hamad, A. Blanco, C. Lopez, S. Vignolini, *ACS Appl. Mater. Interfaces* **2016**, *8*, 31935.

[11] T. Wu, J. Li, J. Li, S. Ye, J. Wei, J. Guo, *J. Mater. Chem. C* **2016**, *4*, 9687.

[12] S. N. Fernandes, P. L. Almeida, N. Monge, L. E. Aguirre, D. Reis, C. L. P. de Oliveira, A. M. F. Neto, P. Pieranski, M. H. Godinho, *Adv. Mater.* **2017**, *29*, 1603560.

[13] K. E. Shopsowitz, H. Qi, W. Y. Hamad, M. J. MacLachlan, *Nature* **2010**, *468*, 422.

[14] J. A. Kelly, M. Giese, K. E. Shopsowitz, W. Y. Hamad, M. J. MacLachlan, *Acc. Chem. Res.* **2014**, *47*, 1088.

[15] M. Schlesinger, M. Giese, L. K. Blusch, W. Y. Hamad, M. J. MacLachlan, *Chem. Commun.* **2015**, *51*, 530.

[16] S. Elazzouzi-Hafraoui, Y. Nishiyama, J.-L. Putaux, L. Heux, F. Dubreuil, C. Rochas, *Biomacromolecules* **2008**, *9*, 57.

[17] J. F. Revol, H. Bradford, J. Giasson, R. H. Marchessault, D. G. Gray, *Int. J. Biol. Macromol.* **1992**, *14*, 170.

[18] X. M. Dong, T. Kimura, J. F. Revol, D. G. Gray, *Langmuir* **1996**, *12*, 2076.

[19] C. Schütz, M. Agthe, A. B. Fall, K. Gordeyeva, V. Guccini, M. Salajkova, T. S. Plivelic, J. P. F. Lagerwall, G. Salazar-Alvarez, L. Bergström, *Langmuir* **2015**, *31*, 6507.

[20] K. Conley, L. Godbout, M. A. T. Whitehead, T. G. M. van de Ven, *Carbohydr. Polym.* **2016**, *135*, 285.

[21] J. P. F. Lagerwall, C. Schütz, M. Salajkova, J. Noh, J. H. Park, G. Scalia, L. Bergström, *NPG Asia Mater.* **2014**, *6*, 80e.

[22] J. F. Revol, L. Godbout, D. G. Gray, *J. Pulp Pap. Sci.* **1998**, *24*, 146.

[23] J. R. Bruckner, A. Kuhnhold, C. Honorato-Rios, T. Schilling, J. P. F. Lagerwall, *Langmuir* **2016**, *32*, 9854.

[24] J.-F. Revol, D. L. Godbout, D. G. Gray, *US 5629055 A* **1997**.

[25] X. Mu, D. G. Gray, *Langmuir* **2014**, *30*, 9256.

[26] G. Guidetti, S. Atifi, S. Vignolini, W. Y. Hamad, *Adv. Mater.* **2016**, *28*, 10042.

[27] S. Beck, J. Bouchard, R. Berry, *Biomacromolecules* **2011**, *12*, 167.

[28] A. G. Dumanli, G. Kamita, J. Landman, H. van der Kooij, B. J. Glover, J. J. Baumberg, U. Steiner, S. Vignolini, *Adv. Opt. Mater.* **2014**, *2*, 646.

[29] J. Pan, W. Hamad, S. K. Straus, *Macromolecules* **2010**, *43*, 3851.

[30] J. H. Park, J. Noh, C. Schütz, G. Salazar-Alvarez, G. Scalia, L. Bergström, J. P. F. Lagerwall, *ChemPhysChem* **2014**, *15*, 1477.

[31] M. Ličen, B. Majaron, J. Noh, C. Schütz, L. Bergström, J. Lagerwall, I. Drevenšek-Olenik, *Cellulose* **2016**, *23*, 3601.

[32] Y. Habibi, T. Heim, R. Douillard, *J. Polym. Sci., Part B: Polym. Phys.* **2008**, *46*, 1430.

[33] B. Frka-Petesic, B. Jean, L. Heux, *Europhys. Lett.* **2014**, *107*, 28006.

[34] B. Frka-Petesic, H. Radavidson, B. Jean, L. Heux, *Adv. Mater.* **2017**, *29*, 1606208.

[35] J. Sugiyama, H. Chanzy, G. Maret, *Macromolecules* **1992**, *25*, 4232.

[36] J.-F. Revol, L. Godbout, X. M. Dong, D. G. Gray, H. Chanzy, G. Maret, *Liq. Cryst.* **1994**, *16*, 127.

[37] X. M. Dong, D. G. Gray, *Langmuir* **1997**, *13*, 3029.

[38] W. J. Orts, L. G. and, R. H. Marchessault, J. F. Revol, *Macromolecules* **1998**, *31*, 5717.

[39] K. Fleming, D. Gray, S. Prasannan, S. Matthews, *J. Am. Chem. Soc.* **2000**, *122*, 5224.

[40] C. D. Edgar, D. G. Gray, *Cellulose* **2001**, *8*, 5.

[41] F. Kimura, T. Kimura, M. Tamura, A. Hirai, M. Ikuno, F. Horii, *Langmuir* **2005**, *21*, 2034.

[42] E. D. Cranston, D. G. Gray, *Sci. Technol. Adv. Mater.* **2006**, *7*, 319.

[43] I. Kvien, K. Oksman, *Appl. Phys. A* **2007**, *87*, 641.

[44] F. Kimura, T. Kimura, *Sci. Technol. Adv. Mater.* **2008**, *9*, 024212.

[45] A. Y. Denisov, E. Kloser, D. G. Gray, A. K. Mittermaier, *J. Biomol. NMR* **2010**, *47*, 195.

[46] G. Song, F. Kimura, T. Kimura, G. Piao, *Macromolecules* **2013**, *46*, 8957.

[47] M. Tatsumi, F. Kimura, T. Kimura, Y. Teramoto, Y. Nishio, *Biomacromolecules* **2014**, *15*, 4579.

[48] M. Tatsumi, Y. Teramoto, Y. Nishio, *Cellulose* **2015**, *22*, 2983.

[49] B. Frka-Petesic, J. Sugiyama, S. Kimura, H. Chanzy, G. Maret, *Macromolecules* **2015**, *48*, 8844.

[50] K. J. De France, K. G. Yager, T. Hoare, E. D. Cranston, *Langmuir* **2016**, *32*, 7564.

[51] D. H. Kim, Y. S. Song, *Carbohydr. Polym.* **2015**, *126*, 240.

[52] D. Li, Z. Liu, M. Al-Haik, M. Tehrani, F. Murray, R. Tannenbaum, H. Garmestani, *Polym. Bull.* **2010**, *65*, 635.

[53] S. Beck, J. Bouchard, G. Chauve, R. Berry, *Cellulose* **2013**, *20*, 1401.

[54] T.-D. Nguyen, W. Y. Hamad, M. J. MacLachlan, *Chem. Commun.* **2013**, *49*, 11296.

[55] T. Hiratani, W. Y. Hamad, M. J. MacLachlan, *Adv. Mater.* **2017**, *110*, 1606083.

[56] S. Vignolini, E. Moyroud, B. J. Glover, U. Steiner, *J. R. Soc., Interface* **2013**, *10*, 20130394.

[57] G. Kamita, B. Frka-Petesic, A. Allard, M. Dargaud, K. King, A. G. Dumanli, S. Vignolini, *Adv. Opt. Mater.* **2016**, *4*, 1950.

[58] A. G. Dumanli, H. M. van der Kooij, G. Kamita, E. Reisner, J. J. Baumberg, U. Steiner, S. Vignolini, *ACS Appl. Mater. Interfaces* **2014**, *6*, 12302.

[59] B. D. Wilts, A. G. Dumanli, R. Middleton, P. Vukusic, S. Vignolini, *APL Photonics* **2017**, *2*, 040801.

[60] J. Majoinen, E. Kontturi, O. Ikkala, D. G. Gray, *Cellulose* **2012**, *19*, 1599.

[61] C. Honorato-Rios, A. Kuhnhold, J. R. Bruckner, R. Dannert, T. Schilling, J. P. F. Lagerwall, *Front. Mater.* **2016**, *3*, 75.

[62] R. M. Parker, B. Frka-Petesic, G. Guidetti, G. Kamita, G. Consani, C. Abell, S. Vignolini, *ACS Nano* **2016**, *10*, 8443.

[63] D. Gray, X. Mu, *Materials* **2015**, *8*, 7873.

[64] D. Gray, *Nanomaterials* **2016**, *6*, 213.

[65] W. Helfrich, *J. Chem. Phys.* **1971**, *55*, 839.

[66] J. P. Hurault, *J. Chem. Phys.* **1973**, *59*, 2068.

[67] O. D. Lavrentovich, D. K. Yang, *Phys. Rev. E* **1998**, *57*, R6269.

[68] T. Ishikawa, O. D. Lavrentovich, *Phys. Rev. E* **2001**, *63*, 030501(R).

[69] M. H. Godinho, P. Pieranski, P. Sotta, *Eur. Phys. J. E: Soft Matter Biol. Phys.* **2016**, *39*, 89.

[70] J. L. Fergason, *Mol. Cryst.* **1966**, *1*, 293.

[71] R. S. Werbowyj, D. G. Gray, *Macromolecules* **1984**, *17*, 1512.

[72] P.-X. Wang, W. Y. Hamad, M. J. MacLachlan, *Nat. Commun.* **2016**, *7*, 11515.

[73] V. Fréedericksz, V. Zolina, *Trans. Faraday Soc.* **1933**, *29*, 919.

[74] P. Pincus, *J. Appl. Phys.* **1970**, *41*, 974.

[75] M. Urbanski, C. G. Reyes, J. Noh, A. Sharma, Y. Geng, V. Subba Rao Jampani, J. P. F. Lagerwall, *J. Phys.: Condens. Matter* **2017**, *29*, 133003.

[76] X. M. Dong, J. F. Revol, D. G. Gray, *Cellulose* **1998**, *5*, 19.

[77] S. Beck, M. Méthot, J. Bouchard, *Cellulose* **2015**, *22*, 101.

1701469 (7 of 7)